Contribution of Magnons to the Magnetic Properties of Fe/GaAs Thin Films

H. El Moussaoui*, M.E. Bentayebi,
A. Fahmi and A. Qachaou

Materials and Subatomic Physics Laboratory, Faculty of Sciences, Ibn Tofail University, B.P. 242, 14000 Kenitra, Morocco

Received: 26.09.2025 & Accepted: 20.04.2026

Doi: 10.12693/APhysPolA.149.169 *e-mail: elmohamid@gmail.com

In this work, we investigate the magnetic properties of the Fe/GaAs superlattice for various thicknesses of the iron magnetic layer. The study was performed within the framework of the Heisenberg model. The excitation spectrum and the magnetization per spin were calculated using the retarded Green function method. We have highlighted that the excitation spectrum splits into two sub-bands of different characteristics, which we have attributed to surface and bulk magnons. Comparison between the calculations and the experimental measurements of magnetization per spin allowed us to obtain a very satisfactory estimation of the exchange integrals. The combined effects of surface anisotropy and dipolar interaction were also investigated through numerical analysis.

topics: exchange integral, magnons, Heisenberg Hamiltonian, magnetic properties

1. Introduction

Interest in quasi-two-dimensional magnetic systems (QTDMS) is primarily due to the fact that they possess different magnetic properties than their three-dimensional (3D) counterparts. This interest in QTDMS also stems from potential applications, such as magnetic storage and sensor technologies [1–3]. In particular, ferromagnetic thin films — especially those deposited on semiconductor substrates — have received considerable attention in recent years because of their interesting physical properties; these systems provide new opportunities for combining magnetic films with the properties of semiconductor materials. Most studies have focused on magnetic $3d$ transition metals (such as Fe) deposited on zinc-blende semiconductors (such as GaAs). This is because the lattice constants of the two layers nearly match one another for this structure [4], and also due to their ready availability either as a bulk substrate material or as an epitaxial thin film.

It is well known that non-zero magnetic anisotropy is necessary for the stability of long-range magnetic order in thin films. The magnetic anisotropy of Fe/GaAs(001) has been intensively studied [5, 6]; it has been shown that the ferromagnetism in this system is stabilized by in-plane uniaxial magnetic anisotropy. In fact, the origin of uniaxial magnetic anisotropy in Fe/GaAs(001) is a combination of the anisotropy of volume and surface/interface [7].

In this work, we present a theoretical study of the contribution of spin waves to the magnetic properties of Fe/GaAs thin films. The present study was performed within the framework of linear spin-wave theory. The Heisenberg Hamiltonian of the system was constructed taking into account the exchange interaction, magneto-crystalline anisotropy, dipolar interactions (D), and surface anisotropy (α). Treating the Hamiltonian using the Green function method allowed us to calculate the excitation spectrum $E(\boldsymbol{k})$ of the studied system. Analysis of the dependence of $E(\boldsymbol{k})$ on the magnetic layer thickness (N) revealed the existence of two populations of magnons having different dynamic properties — these two populations were attributed to bulk and surface magnons. Comparison of our calculated magnetization with experiments allowed us to derive exchange integral values, which are consistent with what is generally found for this type of material. Finally, the combined effects of surface anisotropy and dipolar interaction were also investigated through numerical analysis.

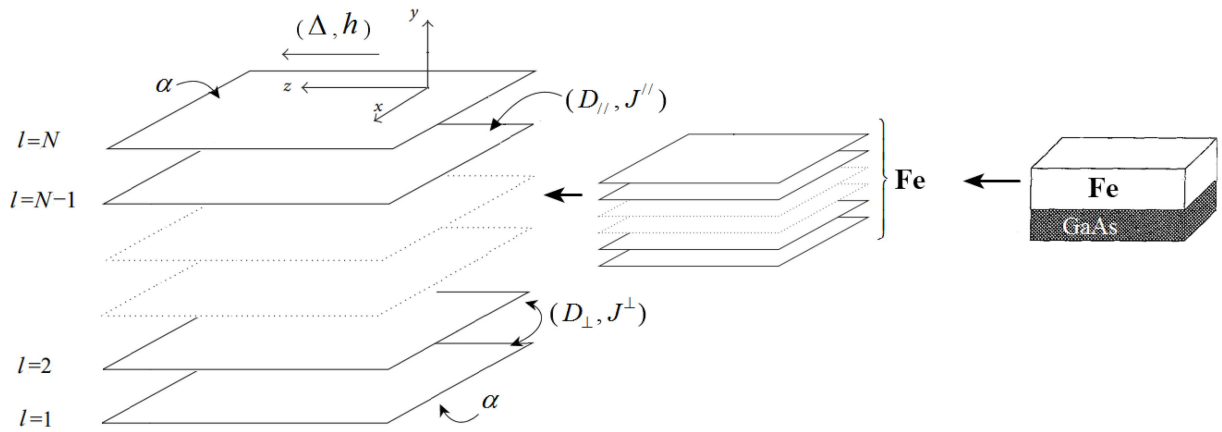

Fig. 1. Schematic figure showing the geometry of the studied system.

2. The spin Hamiltonian

The system considered in this study consists of a single ferromagnetic layer, having a body-centered cubic (bcc) structure, formed from N iron atomic planes, and deposited on a GaAs layer with no spatial repetition. The surfaces of the film are parallel to the (001) plane, and the easy magnetization axis is parallel to the film plane (x–z), as shown in Fig. 1.

The Heisenberg Hamiltonian of the system is given by

$$\mathcal{H} = \mathcal{H}^{ex} + \mathcal{H}^{dip} + \mathcal{H}^{anis} + \mathcal{H}^{chp}. \tag{1}$$

The exchange Hamiltonian is decomposed into two parts, i.e.,

$$\mathcal{H}^{ex} = \mathcal{H}^{ex}_{\parallel} + \mathcal{H}^{ex}_{\perp}. \tag{2}$$

The first part is written as

$$\mathcal{H}^{ex}_{\parallel} = -\sum_{\langle ij\rangle} J^{\parallel}_{ij}\, \boldsymbol{S}_i \cdot \boldsymbol{S}_j = -\sum_{\langle ij\rangle} J^{\parallel}_{ij} \left(S^x_i S^x_j + S^y_i S^y_j + \Delta\, S^z_i S^z_j\right) \tag{3}$$

and represents the exchange interaction between nearest neighboring pairs $\langle ij\rangle$ in the same plane; $J^{\parallel}_{ij}$ is the corresponding exchange integral, and Δ is the magnetocrystalline anisotropy.

The other part represents the exchange interaction between pairs of nearest neighbors $\langle ii'\rangle$ belonging to adjacent planes,

$$\mathcal{H}^{ex}_{\perp} = -\sum_{\langle ii'\rangle} J^{\perp}_{ii'}\, \boldsymbol{S}_i \cdot \boldsymbol{S}_{i'} = -\sum_{\langle ii'\rangle} J^{\perp}_{ii'} \left(S^x_i S^x_{i'} + S^y_i S^y_{i'} + S^z_i S^z_{i'}\right). \tag{4}$$

The expression of dipolar interaction is also composed of two parts, i.e.,

$$\mathcal{H}^{dip} = \mathcal{H}^{dip}_{\parallel} + \mathcal{H}^{dip}_{\perp}. \tag{5}$$

The term $\mathcal{H}^{dip}_{\parallel}$ arises from the first neighbors within the same plane, while $\mathcal{H}^{dip}_{\perp}$ comes from the first neighbors belonging to two adjacent planes, such that

$$\mathcal{H}^{dip}_{\parallel} = \sum_{\langle ij\rangle} \frac{(g\mu_B)^2}{2\, r^3_{ij}} \left[\boldsymbol{S}_i \cdot \boldsymbol{S}_j - 3\frac{(\boldsymbol{S}_i \cdot \boldsymbol{r}_{ij})(\boldsymbol{S}_j \cdot \boldsymbol{r}_{ij})}{r^2_{ij}}\right] = \sum_{\langle ij\rangle} \frac{(g\mu_B)^2}{2\, r^3_{ij}} \left[S^x_i S^x_j + S^y_i S^y_j + S^z_i S^z_j - 3\frac{S^x_i S^x_j \left(r^x_{ij}\right)^2 + S^y_i S^y_j \left(r^y_{ij}\right)^2 + S^z_i S^z_j \left(r^z_{ij}\right)^2}{r^2_{ij}}\right], \tag{6}$$

$$\mathcal{H}^{dip}_{\perp} = \sum_{\langle ii'\rangle} \frac{(g\mu_{\mathrm{B}})^2}{2\, r^3_{ii'}} \left[\boldsymbol{S}_i \cdot \boldsymbol{S}_{i'} - 3\frac{(\boldsymbol{S}_i \cdot \boldsymbol{r}_{ii'})(\boldsymbol{S}_{i'} \cdot \boldsymbol{r}_{ii'})}{r^2_{ii'}}\right] = \sum_{\langle ii'\rangle} \frac{(g\mu_{\mathrm{B}})^2}{2\, r^3_{ii'}} \left[S^x_i S^x_{i'} + S^y_i S^y_{i'} + S^z_i S^z_{i'} - 3\frac{S^x_i S^x_{i'} \left(r^x_{ii'}\right)^2 + S^y_i S^y_{i'} \left(r^y_{ii'}\right)^2 + S^z_i S^z_{i'} \left(r^z_{ii'}\right)^2}{r^2_{ii'}}\right]. \tag{7}$$

The mixed terms $r^{\beta}_{ij} r^{\gamma}_{ij}$ (where $\beta, \gamma \equiv (x, y, z)$, and $\beta \neq \gamma$) are neglected. We adopted an approximation in which the system is considered to be two-dimensional, which is acceptable for very thin films. This approximation leads to $r^y_{ij} = 0$ [8], and consequently, the terms containing $r^y_{ij} r^x_{ij}$ and $r^y_{ij} r^z_{ij}$ are both zero. Due to the inversion symmetry of the crystal, the term containing $r^x_{ij} r^z_{ij}$ is also zero.

The term of the surface anisotropy Hamiltonian is written as

$$\mathcal{H}^{anis} = -\alpha \sum\nolimits'_i (S^y_i)^2. \tag{8}$$

The symbol $\sum_i^{'}$ is restricted to the sites of the surface planes. The last term of the Hamiltonian is given by

$$\mathcal{H}^{chp} = -g\mu_{\mathrm{B}}\, H \sum_i S_i^z = -h \sum_i S_i^z \tag{9}$$

and represents the effect of the applied external magnetic field H along the (Oz) axis.

In order to calculate the excitation spectrum, it is more convenient to carry out two transformations. The first is the linear Holstein–Primakoff transformation [9], which transforms $\boldsymbol{S}$ spin operators into $\hat{a}$ and $\hat{a}^+$ boson operators, i.e.,

$$S_{\boldsymbol{i}}^- = \sqrt{2S}\ \hat{a}_{\boldsymbol{i}}^+, \quad S_{\boldsymbol{i}}^+ = \sqrt{2S}\ \hat{a}_{\boldsymbol{i}}, \quad S_{\boldsymbol{i}}^z = S - \hat{a}_{\boldsymbol{i}}^+ \hat{a}_{\boldsymbol{i}}. \tag{10}$$

The second is the Fourier transformation given by

$$\hat{a}_{\boldsymbol{i}}^+ = \frac{1}{\sqrt{N_\parallel}} \sum_{\boldsymbol{k}} \hat{a}_{\boldsymbol{k},l}^+ \exp(\mathrm{i}\boldsymbol{k}\cdot\boldsymbol{i}_\parallel),$$

$$\hat{a}_{\boldsymbol{i}} = \frac{1}{\sqrt{N_\parallel}} \sum_{\boldsymbol{k}} \hat{a}_{\boldsymbol{k},l} \exp(-\mathrm{i}\boldsymbol{k}\cdot\boldsymbol{i}_\parallel). \tag{11}$$

Here, $N_\parallel$ is the total number of spins in a single plane, $\boldsymbol{k}$ is the two-dimensional in-plane wave vector ($\boldsymbol{k} = (k_x, k_z)$), while l and $\boldsymbol{i}_\parallel$ describe, respectively, the atomic plane index and lattice site in this particular plane, i.e., $\boldsymbol{i}_\parallel$ is the in-plane component of the position vector.

Regarding the k_y component of the wave vector, translation symmetry breaking in the direction perpendicular to the surface of the film prevents waves from propagating in this direction; the plane wave approximation is not acceptable in this direction (i.e., the Fourier transformation is not applicable in this direction). The stationary waves that may occur in this direction can be found by examining the eigenvectors of the Hamiltonian, which can give the intensity of the stationary wave in each atomic plane.

After applying these two transformations to (1), the total Hamiltonian takes the following reduced form

$$\mathcal{H} = \sum_{l,m}^{N} \sum_{\boldsymbol{k}} \Big[A_{lm}(\boldsymbol{k})\, \hat{a}_{\boldsymbol{k},l}^+ \hat{a}_{\boldsymbol{k},m} + \frac{1}{2} B_{lm}(\boldsymbol{k}) \times \Big(\hat{a}_{\boldsymbol{k},l}^+ \hat{a}_{-\boldsymbol{k},m}^+ + \hat{a}_{\boldsymbol{k},l} \hat{a}_{-\boldsymbol{k},m} \Big) \Big], \tag{12}$$

where $\boldsymbol{k} = (k_x, k_z)$ and A_{lm} and B_{lm} are obtained for the atomic planes l and m ($1 \le l \le N$ and $1 \le m \le N$). They are defined as

$$\begin{aligned} A_{lm}(\boldsymbol{k}) = S\Bigg\{ \Bigg[4J^\parallel \big(\Delta - \Sigma(\boldsymbol{k})\big) + D_\parallel \Bigg(\frac{1}{2} - \frac{3}{2} \Bigg(\frac{r_{\delta_\parallel}^x}{r_{\delta_\parallel}} \Bigg)^2 \Bigg) \Sigma(\boldsymbol{k}) - \Bigg(\frac{1}{2} - 3 \Bigg(\frac{r_{\delta_\parallel}^z}{r_{\delta_\parallel}} \Bigg)^2 \Bigg) \Bigg] + h - \alpha\big(\delta_{l,1} + \delta_{l,N}\big) \\ + \Bigg[4J^\perp + D_\perp \Bigg(3 \Bigg(\frac{r_{\delta_\perp}^z}{r_{\delta_\perp}} \Bigg)^2 - 2 \Bigg) \Bigg] \big(2 - \delta_{l,1} - \delta_{l,N} \big) \Bigg\}\, \delta_{l,m} - S \Bigg[4J^\perp - D_\perp \Bigg(1 - \frac{3}{8} \frac{(r_{\delta_\perp}^x)^2 + (r_{\delta_\perp}^y)^2}{r_{\delta_\perp}^2} \Bigg) \Bigg] \Lambda(\boldsymbol{k}) \\ \times \big(\delta_{l,m-1} + \delta_{l,m+1} \big), \end{aligned} \tag{13}$$

$$B_{lm}(\boldsymbol{k}) = S \Bigg(-\frac{3}{2} D_\parallel \Bigg(\frac{r_{\delta_\parallel}^x}{r_{\delta_\parallel}} \Bigg)^2 \Sigma(\boldsymbol{k}) + \alpha\big(\delta_{l,1} + \delta_{l,N}\big) \Bigg)\, \delta_{l,m} - \frac{3}{4} S D_\perp \Bigg(\frac{(r_{\delta_\perp}^x)^2 - (r_{\delta_\perp}^y)^2}{r_{\delta_\perp}^2} \Bigg)^2 \Lambda(\boldsymbol{k}) \big(\delta_{l,m-1} + \delta_{l,m+1} \big), \tag{14}$$

where $\boldsymbol{r}_{\delta_\parallel} = (r_{\delta_\parallel}^x, r_{\delta_\parallel}^y, r_{\delta_\parallel}^z)$ denotes the distances between first neighbors in the same plane, while $\boldsymbol{r}_{\delta_\perp} = (r_{\delta_\perp}^x, r_{\delta_\perp}^y, r_{\delta_\perp}^z)$ denotes the distances between first neighbors belonging to two different planes. The dipolar interaction constants are $D_\parallel = (g\mu_{\mathrm{B}})^2 / ||r_{\delta_\parallel}||^3$ and $D_\perp = (g\mu_{\mathrm{B}})^2 / ||r_{\delta_\perp}||^3$, and $\delta_{i,j}$ represents the Kronecker delta. The variable Σ is defined as $\Sigma(\boldsymbol{k}) = [\cos(ak_x) + \cos(ak_z)]/2$, and Λ is given by $\Lambda(\boldsymbol{k}) = \cos(ak_x/2)\cos(ak_z/2)$, where a is the lattice parameter.

The excitation spectrum is obtained by diagonalizing (12) using the Green functions defined by

$$G_{l,m} = \langle\langle \hat{a}_{\boldsymbol{k},l}, \hat{a}_{\boldsymbol{k},m}^+ \rangle\rangle, \quad G_{l,m}^{'} = \langle\langle \hat{a}_{-\boldsymbol{k},l}^+, \hat{a}_{\boldsymbol{k},m}^+ \rangle\rangle, \tag{15}$$

for l and $m \in \{1, \ldots, N\}$.

The dynamics of $G_{l,m}$ and $G_{l,m}^{'}$ are governed by the equations of motion leading to the following two expressions

$$\begin{cases} E\langle\langle \hat{a}_{\boldsymbol{k},l} \big| \hat{a}_{\boldsymbol{k},m}^+ \rangle\rangle = \\ \quad \frac{1}{2\pi} \langle [\hat{a}_{\boldsymbol{k},l}, \hat{a}_{\boldsymbol{k},m}^+] \rangle + \langle\langle [\hat{a}_{\boldsymbol{k},l}, \mathcal{H}] \big| \hat{a}_{\boldsymbol{k},m}^+ \rangle\rangle, \\ E\langle\langle \hat{a}_{-\boldsymbol{k},l}^+ \big| \hat{a}_{\boldsymbol{k},m}^+ \rangle\rangle = \\ \quad \frac{1}{2\pi} \langle [\hat{a}_{-\boldsymbol{k},l}, \hat{a}_{\boldsymbol{k},m}^+] \rangle + \langle\langle [\hat{a}_{-\boldsymbol{k},l}, \mathcal{H}] \big| \hat{a}_{\boldsymbol{k},m}^+ \rangle\rangle. \end{cases} \tag{16}$$

Note that on the right-hand side, a higher-order Green function appears, which leads to another equation of motion of even higher-order Green function, and so forth. In this way, an exact, infinite hierarchy of equations of motion is generated. In our work, we limited ourselves to the first-order approximation.

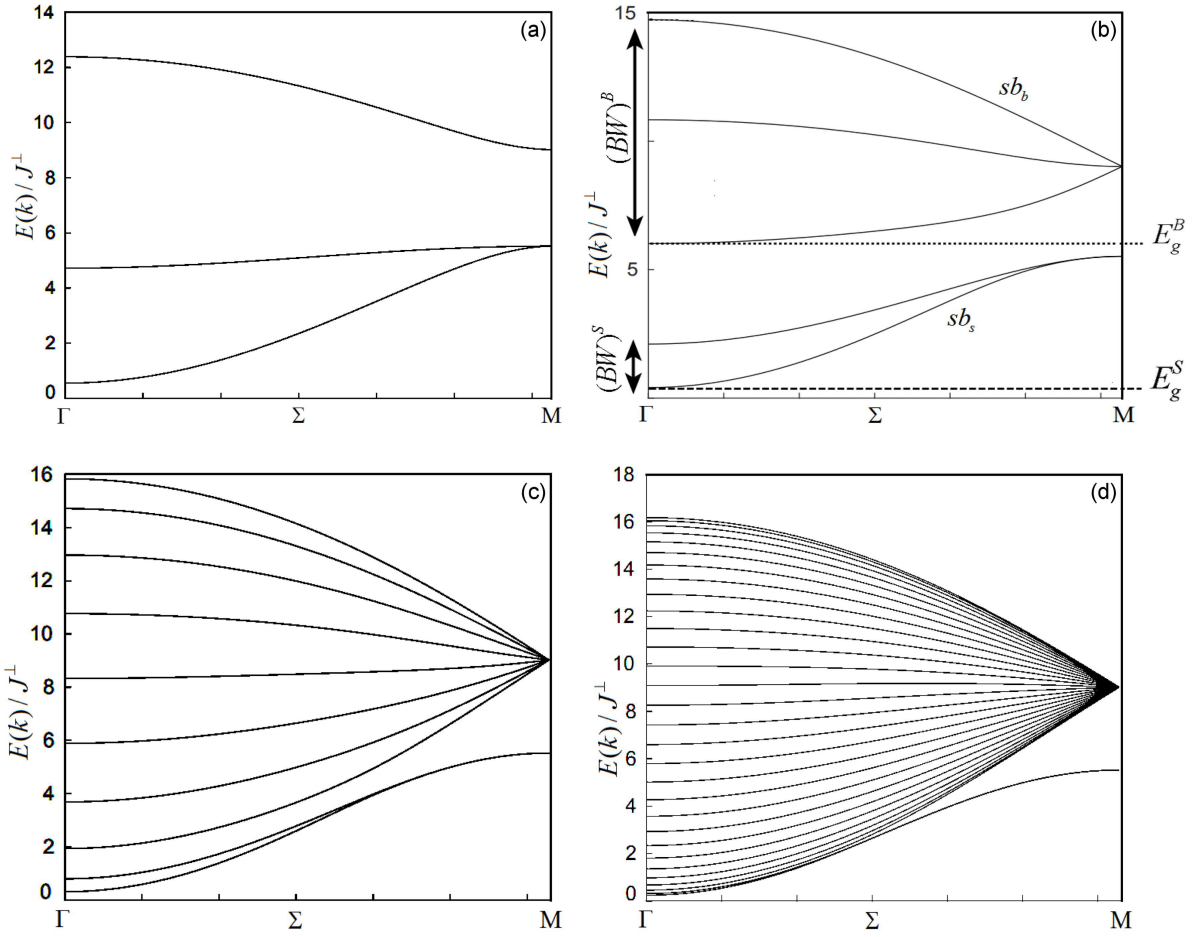

Fig. 2. Excitation spectra of the superlattices Fe/GaAs for: (a) $N = 3$, (b) $N = 5$, (c) $N = 10$, (d) $N = 30$, where $J^{\perp} = 10J^{\parallel} = 10$ K, $S = 1$, $h = 0.05$ K, and $\Delta = 1.3$.

These equations of motion lead to a system of $2N$ coupled equations, which can be represented in the following matrix form

$$\begin{pmatrix} \mathbb{A} - E & \mathbb{B} \\ -\mathbb{B} & -\mathbb{A} - E \end{pmatrix} \begin{pmatrix} \mathbb{G} & 0 \\ \mathbb{G}' & 0 \end{pmatrix} = -\frac{1}{2\pi} \begin{pmatrix} 1 & 0 \\ 0 & 0 \end{pmatrix}. \tag{17}$$

Here, $\mathbb{A}$ and $\mathbb{B}$ are the matrices of $N \times N$ order given by (13) and (14).

3. Exchange interaction

Since the effect of the exchange interaction is more important than that of the surface anisotropy and dipolar interactions in $3d$ transition metals like iron, in this section we have confined ourselves to the study of this effect exclusively ($D = \alpha = 0$). The Hamiltonian (12) then takes the reduced form

$$\mathcal{H} = \sum_{lm}^{N} \sum_{\boldsymbol{k}} A_{lm}(\boldsymbol{k})\ \hat{a}^{+}_{\boldsymbol{k},l}\, \hat{a}_{\boldsymbol{k},m}. \tag{18}$$

3.1. Excitation spectrum

The spin wave energies $E(\boldsymbol{k})$ are obtained in the same way as those of previously studied systems [10, 11], namely by solving (17), which leads to

$$\mathrm{Det}\Big[\mathbb{A} - E\,\mathbb{I}\Big] = 0. \tag{19}$$

By solving numerically (19), we obtained the excitation spectrum presented in Fig. 2.

Figure 2 shows that for weak values of N (3, 5, and 10), the number of obtained modes is equal to the number of atomic planes of the magnetic layer; this is in agreement with what we have found in previous works [12–17]. In contrast, for higher values of N, the number of modes differs from the number of magnetic planes; in fact, for $N = 30$, there are only 29 modes, as shown in Fig. 2d. This is due to the lower modes becoming degenerate for a wide range of the first Brillouin zone.

We also note that a non-zero lower energy level exists in the spectrum near $\boldsymbol{k} = (0, 0)$, for all values of N. This allows us to define a threshold or gap

energy (E_g) that represents the lowest energy necessary for the creation of a spin wave in the studied system. The study of E_g is relevant because it provides information about the degree of magnetic stability of a given system; for example, when $E_g = 0$, the long-range magnetic order vanishes [18, 19].

We notice as well that the energy modes in the excitation spectrum can be classified into two groups or bands. The first one is constituted by the two modes corresponding to the lowest energy values, and the second is constituted by the remaining $(N-2)$ modes. We also remark that when the number N of magnetic planes increases, the width of the first band $(BW)^S$ remains almost invariant, while the bandwidth of the second $(BW)^B$ grows increasingly. This suggests that the first group is due to surface effects, while the higher-energy band is due to volume.

It can also be noted that the obtained shape of the excitation spectrum differs from that found in our earlier study [20]. In fact, in this previous study, the shape of the excitation spectrum was such that each mode was just a translation of another along the energy axis. This may be due to the crystallographic structure being a simple cube. In this particular geometry, each site in a given atomic plane has its out-of-plane neighbors perpendicular to the plane; this results in the non-diagonal elements of the Hamiltonian matrix becoming independent of the wave vector $\boldsymbol{k}$.

In contrast, in the present work, we study a more realistic bcc structure. This specific geometry structure leads to off-diagonal elements of the Hamiltonian that depend on the value of the wave vector $\boldsymbol{k}$, which translates into the emergence of two distinct sub-bands, where the modes of each sub-band become completely degenerate at the edge of the Brillouin zone; a similar effect is observed in a previous study [21].

The quantitative properties, such as the exact position of the modes in the spectrum, can depend on the type of substrate since the latter can impact the anisotropy and exchange in the magnetic layer. In fact, in our specific case, it is well known that when a thin iron layer is deposited on GaAs, the system usually presents an in-plane easy axis of magnetization [22–24] with a strong uniaxial anisotropy [25–27]. This strong anisotropy affects the magnon spectrum since it strengthens the gap of magnon creation; this is shown with more clarity through the following formula [11] (which is valid as a first approximation if we consider only the dominant effect of the exchange interaction)

$$E_g = 8\,SJ^{\parallel}\Big(\Delta - 1\Big) - 2\,SJ^{\perp}. \tag{20}$$

From (20), it can be seen that Δ and E_g have the same sign, which indicates that when the anisotropy increases, the gap energy increases too, leading to a stronger magnetic order, i.e., the creation of spin waves becomes increasingly difficult,

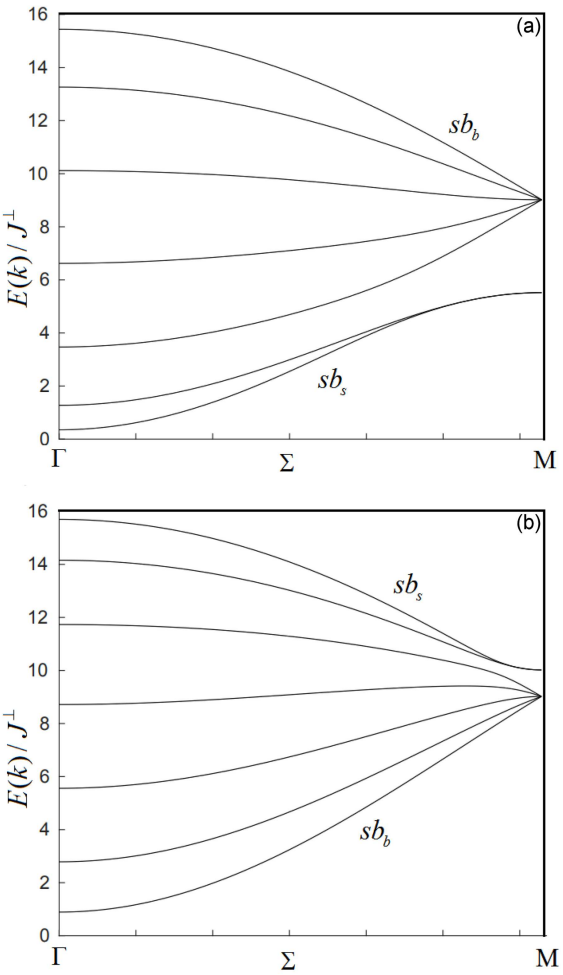

Fig. 3. Excitation spectra of the superlattices Fe/GaAs for: (a) $\alpha = 5$ K, (b) $\alpha = -50$ K, where $N = 7$, $J^{\perp} = 10J^{\parallel} = 10$ K, $S = 1$, $h = 0.05$ K, and $\Delta = 1.3$.

and this tendency is accentuated when the Fe layer is deposited on GaAs since this deposition usually strengthens the anisotropy Δ of the iron layer.

On the other hand, some qualitative properties (such as the splitting of the spectrum into two subbands) do not necessarily depend on the type of substrate. A multitude of studies of magnetic layers deposited on diverse non-magnetic substrates report splitting of the excitation spectrum into two distinct sub-bands attributed to surface and bulk magnons [28–31]. The splitting of the spectrum is most likely an intrinsic property of the magnetic layer that results from its crystallographic structure.

Figure 3 represents the excitation spectrum of a magnetic thin film made of $(N = 7)$ atomic planes for two values of the surface anisotropy. The spectra $E(\boldsymbol{k}, \alpha)$ is obtained by adding its corresponding term

$$E(\boldsymbol{k}, \alpha) = E(\boldsymbol{k}) - \alpha\left(\delta_{l,1} + \delta_{l,N}\right). \tag{21}$$

TABLE I

Values of the energy gaps E_g^S and E_g^B as a function of N.

	N			
	3	5	10	30
$E_g^B/J^\perp$	12.39	6.02	1.93	0.45
$E_g^S/J^\perp$	0.54	0.41	0.3	0.24

TABLE II

Values of τ_S, τ_B, and (τ_B/τ_S) versus N.

N	τ_B [s]	τ_S [s]	τ_B/τ_S
3	2.24×10^{-13}	1.18×10^{-10}	1.9×10^{-3}
5	9.5×10^{-13}	2×10^{-10}	4.75×10^{-3}
10	9.24×10^{-12}	3.8×10^{-10}	2.43×10^{-2}
30	1.7×10^{-10}	6×10^{-10}	2.8×10^{-1}

We notice that the variation of α affects more the sub-band constituted of 2 modes (sb_s) in comparison with the one containing $N-2$ modes (sb_b). This remark is in agreement with the analysis above, attributing these two sub-bands to surface and volume magnons, respectively.

We also note that for high values of $|\alpha|$ (in our case $\alpha = -50$ K), the surface modes appear above the bulk ones (Fig. 3b), which suggests that, in this case, the creation of magnons has a higher energy cost at the surface of the system.

In fact, this is consistent with findings of a previous study by M. Mehdioui et al. [10], which emphasizes the existence of two populations of magnons possessing distinct dynamic characteristics. In this cited study, the surface sub-band appears only above the bulk sub-band, whereas the present work gives a more complete physical picture by showing that the surface modes can also appear under the bulk ones for small values of $|\alpha|$ (Fig. 3a) and that the relative position of these two sub-bands depends, in general, on the surface physical properties of the surface, particularly the surface anisotropy.

To better understand the creation and dynamics of the two magnon populations corresponding to the two sub-bands, we will study two characteristic factors of these sub-bands, namely the magnon creation gaps (E_g^S and E_g^B) of the surface and bulk, respectively, and their associated lifetimes τ_S and τ_B.

3.2. Energy gap and lifetime of created magnons

3.2.1. Energy gaps E_g^S and E_g^B

We directly measured the gap energies E_g^S and E_g^B presented by the excitation spectrum (Fig. 2). The obtained values are gathered in Table I.

We observe that both E_g^B and E_g^S decrease as the number of magnetic layers (N) increases. We also remark that the decrement in E_g^B is greater than that in E_g^S; this difference in the sensitivity of the two gaps to the thickness of the magnetic layer may be due to the difference in coordination between an atom belonging to the surface and another situated in the internal atomic planes. In fact, in the first case, every atom is surrounded by 8 first neighbors, while in the second, an atom is surrounded by 12 first neighbors.

At the limit of large N, E_g^B tends towards values very close to E_g^S, suggesting that the bulk and surface sub-bands can overlap for large values of N. The spacing $\Delta E_g = |E_g^B - E_g^S|$ can serve as an indication of whether the system belongs to the thin film category or to the bulk one; the value of ΔE_g is important for thin layers, while it is negligible (or zero) for thick layers.

3.2.2. Magnon lifetimes τ_S and τ_B

In order to further investigate the characteristics of these two populations of magnons, we attempted to track their dynamics through the study of their lifetimes τ_S and τ_B.

Following a reasoning similar to what we have done in previous studies [32], we estimated the lifetime of magnons as follows

$$\tau^{-1} = \frac{2\pi}{\hbar} E_g^2 \, D_d(E_F), \tag{22}$$

where $D_d(E_F) \simeq 4.16$ eV^{-1} is the iron density of states at the Fermi level. If we assume, as a first approximation, that the densities of states $|D_d(E_F)|_{S,B}$ remain very close, we can express the ratio of lifetimes τ_S and τ_B in the following form

$$\frac{\tau_B}{\tau_S} \simeq \frac{|E_g^S|^2}{|E_g^B|^2}. \tag{23}$$

Based on (22) and (23) and the values of the gap energies in Table I, we created Table II, bringing together the values of τ_S, τ_B, and τ_B/τ_S for different values of N.

Table II shows that as the thickness of the magnetic layer increases, the lifetime of the bulk magnons (τ_B) also increases, while the lifetime of the surface magnons remains almost unchanged. This suggests that the contribution of bulk magnons to the magnetic properties of the studied system is more significant for the thicker magnetic layers. Table II also shows that the ratio τ_B/τ_S increases when N increases; this ratio is of the order of about 1/1000 for a layer of $N = 3$ atomic planes, which means that a spin wave created in the bulk disappears a thousand times faster than another created at the surface of the magnetic layer. This allows us to conclude that for thin magnetic layers, the creation of surface magnons is favored. In contrast, for

thick magnetic layers, the values of τ_S and τ_B become relatively comparable (for $N = 30$, the ratio τ_B/τ_S reaches a value of 0.28). This clearly highlights the difference in terms of dynamics between the two populations of magnons.

Our results agree with those obtained by M. Karam et al. [21], also showing that the lifetime of surface magnons is generally (exchange alone) greater than that of bulk magnons and that the bulk magnon lifetime increases with magnetic layer thickness. In comparison to that study, which concentrates on the effect of the surface anisotropy, our study, although following similar reasoning, also hints at the important role of the reduction in coordination at the surfaces of the ferromagnetic film (see Sect. 3.2.1); in fact, this factor can cause the emergence of surface modes even if the value of the surface anisotropy is weak. In addition, the present work provides direct and explicit values of the ratio of lifetimes of the two populations of magnons — this allows for an easier and more intuitive evaluation of the relative dynamics of each magnon population.

3.3. Comparison between the calculated and measured magnetization

The total magnetization of a solid at a temperature T is given by

$$M_Z(T) = g\mu_{\mathrm{B}}\ \langle S^z\rangle_T = g\mu_B\left[\langle S\rangle - \sum\nolimits_{\boldsymbol{k}}\langle \hat{a}^+_{\boldsymbol{k}}\hat{a}_{\boldsymbol{k}}\rangle\right]. \tag{24}$$

For a superlattice made of N atomic planes, we have

$$\langle \hat{a}^+_{\boldsymbol{k},l}\hat{a}_{\boldsymbol{k},l}\rangle = \left[\exp\left(\frac{E_l(\boldsymbol{k})}{k_{\mathrm{B}}T}\right) - 1\right]^{-1}, \tag{25}$$

with $l = 1, \ldots, N$.

The expression of the magnetization per spin of the superlattice can then be expressed as

$$m_z(T) = \frac{\langle S^z\rangle}{S} =$$

$$1 - \frac{1}{S\,N}\frac{s}{(2\pi)^2}\sum_{l=1}^{N}\int_{\mathrm{BZ}} \mathrm{d}k_x\,\mathrm{d}k_z\ \langle \hat{a}^+_{\boldsymbol{k},l}\,\hat{a}_{\boldsymbol{k},l}\rangle =$$

$$1 - \frac{1}{S\,N}\sum_{l=1}^{N}\frac{s}{(2\pi)^2}\int \frac{\mathrm{d}k_x\,\mathrm{d}k_z}{\exp\left(\frac{E_l(\boldsymbol{k})}{k_{\mathrm{B}}T}\right) - 1}, \tag{26}$$

where s is the surface of an elementary cell, and k_{B} is the Boltzmann constant.

Using (26) allowed us to compare our calculated magnetization $m_z(H)_{cal}$ with the experimental measurements $m_z(H)_{exp}$, as shown in Fig. 4.

Figure 4 presents the variation of the magnetization of the studied thin film versus the applied magnetic field. We note that when the value of the magnetic field rises, the magnetization increases rapidly, and then the increment of the magnetization as a function of H becomes gradually smaller until the magnetization stagnates (reaches a saturation value). In fact, when the magnetic field strengthens, it aligns more and more magnetic moments in its direction until all the moments of the system become aligned. The agreement reached between our calculated magnetization

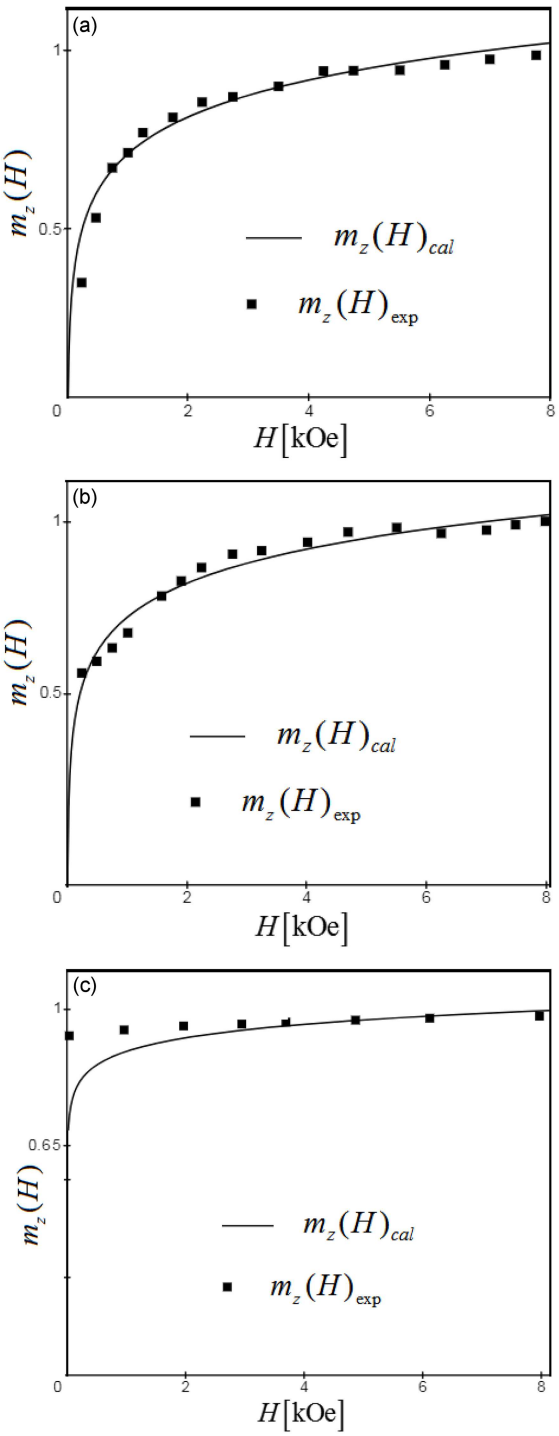

Fig. 4. Variation of the magnetization of the superlattice Fe/GaAs as a function of the applied magnetic field for: (a) $N = 3$, (b) $N = 4$, (c) $N = 5$.

$m_z(H)_{cal}$ from (26) (solid lines in Fig. 4) and the experimental magnetization $m_z(H)_{exp}$ at $T = 10$ K (symbols) [33] is very good; this allowed us to deduce the exchange integrals values (Table III) of the system, and these deduced exchange values are coherent with what is usually found for this type of materials [34, 35].

Although the GaAs substrate has a significant effect on the properties of the system, this effect was not directly addressed in the present model, i.e., there is no parameter in the Hamiltonian that is attributed to the exclusive effect of the GaAs substrate, since the approach of this study is a semi-empirical one. In fact, the GaAs substrate effect was implicitly captured by adjusting theoretical and experimental magnetization, which allowed us to deduce parameters such as $J^{\parallel}$ and Δ, which carry in their values the contribution of the GaAs substrate indirectly. Even though the present work did not focus on quantifying this contribution, it still confirms that the model used can describe the spin-wave behavior in magnetic layers (such as Fe) deposited on the GaAs substrate. A precise determination of the contribution of the substrate interface to the magnetic properties of the system necessitates using sophisticated electronic structure calculations based on *ab initio* methods, such as density functional theory (DFT). However, this is beyond the scope of the present study and will be addressed in future work.

4. Combined effects of surface anisotropy and dipolar interaction

The combined effects of dipolar interactions (D) and surface anisotropy (α) play an important role in the stability of the long-range magnetic order of quasi-two-dimensional systems [36–39]. However, the analytical expressions of the excitation spectrum $E(\boldsymbol{k})$ and consequently of the magnetization per spin $m_z(T)$ of the system become too difficult to obtain directly when the two factors above (D and α) are introduced, especially for large numbers of magnetic planes ($N \gg 1$). To address the general case of a superlattice containing any number of atomic planes, we will proceed numerically starting from (26).

In Fig. 5, we present the thermal variation of the magnetization ratio,

$$\rho_N(T,R) = \frac{m_z(T, R \neq 1)}{m_z(T, R = 1)}, \tag{27}$$

where $R = D/\alpha$. Thus, ρ_N represents the magnetization for the case $D \neq \alpha$ relative to that of the reference case $D = \alpha$, in which the dipolar interaction and surface anisotropy have equal strength. We note that, for temperatures below a threshold value $T < T_s(N)$, these two parameters, i.e., α and D, have no effect, since the curves representing the magnetization ratio for ($D \gg \alpha$) and ($D \ll \alpha$) are identical, which indicates that the effects of surface anisotropy and dipolar interaction are mutually compensated in this temperature range.

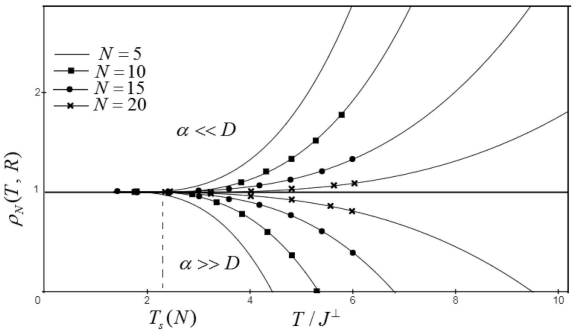

Fig. 5. Thermal variation of the magnetization ratio $\rho_N(T,R)$, with $D = (D_{\parallel} + D_{\perp})/2$.

TABLE III

Deduced values of the exchange integrals for different N, with $J^{\perp} = 10J^{\parallel}$ and $S = 1$.

N	$J^{\parallel}$ [K]	Δ
3	17	1.008
4	19	1.03
5	20	1.05

Furthermore, we observe that the threshold temperature $T_s(N)$ increases when the number of atomic planes N constituting the studied magnetic layer rises; this indicates that the effects of these interactions are more important for the finest magnetic layers. We also note that when the contribution of the surface anisotropy is most significant ($R < 1$), the magnetization decreases, while in the case where the contribution of the dipolar interactions is dominant ($R > 1$), the magnetization increases. In fact, dipolar interactions tend to align the magnetic moments parallel to the plane of the film, while surface anisotropy orients them in a perpendicular direction. This may be the cause of the antagonistic character of these two interactions.

We also notice that the effect of the $R = \alpha/D$ ratio on the magnetization ratio seems more pronounced when $R > 1$ than in the reverse case — this is revealed by the asymmetry, relative to the axis $\rho = 1$, of any two $\rho_N(T,R)$ curves with ($R > 1$ and $R < 1$). This asymmetry shows that the surface anisotropy α has a more significant effect in these ultrathin films. This fact can be related to the surface-to-volume ratio in these quasi-two-dimensional systems (the surface-to-volume ratio becomes greater for thinner layers, which favors α over D). We remark that this asymmetry itself is not independent of the magnetic layer thickness; it becomes more accentuated for thinner films (small N values). This remark will be further analyzed in upcoming studies.

5. Conclusions

In this work, we studied the spin wave contribution to the magnetic properties of the Fe/GaAs thin films for various thicknesses of the (Fe) layer. We established the corresponding Heisenberg Hamiltonian, taking into account the direct exchange interaction, the anisotropy, and the dipolar interactions. The Hamiltonian was diagonalized using the technique of Green functions.

We found that, for the very thin films, the number of modes in the excitation spectrum $E(\boldsymbol{k})$ is equal to the number N of atomic planes of the magnetic layer. We have also demonstrated the existence of an energy gap for magnon creation that depends on the thickness of the studied magnetic layer. We have also highlighted that $E(\boldsymbol{k})$ presents two sub-bands of different characteristics, which we have attributed to bulk and surface magnons. We have shown as well that these two populations of magnons exhibit very different dynamic properties, which is particularly prominent when the studied magnetic film becomes thinner. The agreement between calculated and measured magnetization is very satisfactory, which allowed us to determine the values of the exchange integrals of the studied system. The obtained values are in agreement with those usually found for this type of material. The study of the combined effects of surface anisotropy and dipolar interaction, reported at the end, emphasized the important role that the dipolar interaction plays in the stabilization of the magnetic order in this type of quasi-two-dimensional systems.

References

[1] S.M. Yakout, *J. Supercond. Nov. Magn.* **33**, 2557 (2020).

[2] A.V. Kimel, M. Li, *Nat. Rev. Mater.* **4**, 189 (2019).

[3] A.V. Kimel, A.M. Kalashnikova, A. Pogrebna, A.K. Zvezdin, *Phys. Rep.* **852**, 1 (2020).

[4] P.K. Muduli, J. Herfort, H.-P. Schönherr, L. Däweritz, K.H. Ploog, *Appl. Phys. A* **81**, 901 (2005).

[5] R. Moosbühler, F. Bensch, M. Dumm, G. Bayreuther, *J. Appl. Phys.* **91**, 8754 (2002).

[6] R. Zuberek, K. Fronc, A. Szewczyk, M.U. Gutowska, H. Szymczak, M.R.J. Gibbs, *Czechslov. J. Phys.* **52**, A169 (2002).

[7] B. Kardasz, E.A. Montoya, C. Eyrich, E. Girt, B. Heinrich, *J. Appl. Phys.* **109**, 07D337 (2011).

[8] M.G. Pini, P. Politi, R.L. Stamps, *Phys. Rev. B* **72**, 014454 (2005).

[9] T. Holstein, H. Primakoff, *Phys. Rev.* **58**, 1098 (1940).

[10] M. Mehdioui, A. Fahmi, H. Lassri, M. Fahoume, A. Qachaou, *J. Magn. Magn. Mater.* **352**, 107 (2014).

[11] M.E. Bentayebi, A. Qachaou, M. Lhrach, A. Fahmi, *J. Supercond. Nov. Magn.* **27**, 2879 (2014).

[12] T. Balashov, P. Buczek, L. Sandratskii, A. Ernst, W. Wulfhekel, *J. Phys. Condens. Matter* **26**, 39 (2014).

[13] R. Vollmer, M. Etzkorn, P.S.A. Kumar, H. Ibach, J. Kirschner, *Phys. Rev. Lett.* **91**, 147201 (2003).

[14] S. Mamica, *Adv. Condens. Matter Phys.* **2015**, 17 (2015).

[15] S. Mamica, R. Józefowicz, H. Puszkarski, *Acta Phys. Pol. A* **94**, 79 (1998).

[16] H. Puszkarski, J.C.S. Lévy, S. Mamica, *Phys. Lett. A* **246**, 347 (1998).

[17] S. Mamica, *Eur. Phys. J. B* **87**, 293 (2014).

[18] R.-K. Qiu, P.-P. Song, Z.-D. Zhang, *J. Magn. Magn. Mater.* **321**, 3031 (2009).

[19] P. Aleshkevych, M. Baran, H. Szymczak, *Acta Phys. Pol. A* **106**, 593 (2004).

[20] H. Elmoussaoui, A. Fahmi, M. Fahoume, A. Qachaou, *Phys. E Low-Dimen. Syst. Nanostruct.* **57**, 149 (2014).

[21] M. Karam, A. Fahmi, M. Fahoume, M. Lhrach, A. Qachaou, *J. Low Temp. Phys.* **214**, 442 (2024).

[22] B. Lépine, C. Lallaizon, S. Ababou et al., *J. Cryst. Growth* **201–202**, 702 (1999).

[23] Y. Chye, V. Huard, M.E. White, P.M. Petroff, *Appl. Phys. Lett.* **80**, 449 (2002).

[24] P.K. Muduli, J. Herfort, H.-P. Schönherr, K.H. Ploog, *J. Appl. Phys.* **97**, 123904 (2005).

[25] W. Kipferl, M. Dumm, M. Rahm, G. Bayreuther, *J. Appl. Phys.* **93**, 7601 (2003).

[26] P.K. Muduli, J. Herfort, H.-P. Schönherr, K.H. Ploog, *J. Magn. Magn. Mater* **320**, 2835 (2008).

[27] W. Kipferl, M. Sperl, T. Hagler, R. Meier, G. Bayreuther, *J. Appl. Phys.* **97**, 10B313 (2005).

[28] H. Salhi, K. Chafai, O. Msieh, H. Lassri, K. Benkirane, M. Abid, L. Bessais, E.K. Hlil, *J. Supercond. Nov. Magn.* **24**, 1379 (2011).

[29] C. Pinettes, C. Lacroix, *J. Magn. Magn. Mater* **166**, 59 (1997).

[30] P. Politi, M.G. Pini, M. Macció, A. Rettori, *Phys. Rev. B* **46**, 8312 (1992).

[31] R. Vollmer, M. Etzkorn, P.S. Anil Kumar, H. Ibach, J. Kirschner, *J. Appl. Phys.* **95**, 7435 (2004).

[32] N. Ait Labyad, A. Qachaou, A. Fahmi, M. Fahoume, M. Lharch, *Appl. Phys. A* **128**, 710 (2022).

[33] J. Herfort, W. Braun, A. Trampert, H.-P. Schoönherr, K.H. Ploog, *Appl. Surf. Sci.* **237**, 181 (2004).

[34] K. Benkirane, R. Elkabil, A. Hamdoun, M. Lassri, M. Abid, H. Lassri, R. Krishnan, *Phys. B Condens. Matter* **353**, 46 (2004).

[35] M. Macció, M.G. Pini, P. Politi, A. Rettori, *Phys. Rev. B* **46**, 8276 (1992).

[36] T.J. Hicks, T. Keller, A.R. Wildes, *J. Magn. Magn. Mater.* **474**, 512 (2019).

[37] M. Hummel, F. Schwabl, *Phys. Rev. B* **63**, 094425 (2001).

[38] E.Y Vedmedenko, A. Ghazali, J.-C.S. Lévy, *Surf. Sci.* **402–404**, 391 (1998).

[39] S. Mamica, J.-C. S. Lévy, M. Krawczyk, P. Depondt, *J. Appl. Phys.* **112**, 043901 (2012).